Proceedings of the International MultiConference of Engineers and Computer Scientists 2015 Vol II,
IMECS 2015, March 18 - 20, 2015, Hong Kong

Ultrasonically Driven Antibubbles Encapsulated by Newtonian Fluids for Active Leakage Detection

Kristoffer Johansen, Spiros Kotopoulis, and Michiel Postema

***Abstract*—An antibubble consists of a liquid droplet, surrounded by a gas, often with an encapsulating shell. Antibubbles of microscopic sizes suspended in fluids are acoustically active in the ultrasonic range. In this study, a Rayleigh-Plesset-like model is derived for micron-sized antibubbles encapsulated by Newtonian fluids. The theoretical behaviour of an encapsulated antibubble is compared to that of an antibubble without an encapsulating shell, a free gas bubble, and an encapsulated gas bubble. Antibubbles, with droplet core sizes in the range of 60–90% of the equilibrium antibubble inner radius were studied. Acoustic pressures of 100 kPa and 300 kPa were studied. The antibubble resonance frequency, the phase difference of the radial oscillations with respect to the incident acoustic pulse, and the presence of higher harmonics are strongly dependent of the core droplet size. The contribution to the radial dynamics from a zero-thickness shell is negligible for the bubble size studied, at high acoustic amplitudes, antibubbles oscillate highly nonlinearly independent of core droplet size. This may allow for active leakage detection using harmonic imaging methods.**

***Index Terms*—Active leakage detection, Antibubble, Bubble resonance, Microbubble, Nonlinear dynamics**

I. Introduction

RECENTLY, it has been proposed to locate offshore hydrocarbon production facilities subsea instead of at the surface [1]. Locating production facilities subsea is not only to decrease cost, but also to initiate production of hydrocarbons at greater depths. Furthermore, several of the new production fields in the Northern Hemisphere are placed in Arctic climates. Therefore, low temperatures are becoming a major challenge. Hence, using subsea production plants to extract hydrocarbon in such region solves several problems. However, when establishing subsea production plants, it is essential to secure appropriate maintenance surveillance. An up-and-coming method is ultrasound-based active leakage detection [2]. This is achieved by studying the composition of sound scattered back to the ultrasound source. Knowing that gas bubbles scatter sound more effectively than solid objects or liquids, it is possible to differentiate them [2]. In oil exploration, the flow coming up from the reservoir is a mixture of water, oil and gas. Therefore it can be assumed that leaks from subsea production facilities inhibit the three components necessary for the production of antibubbles [3]: gas, a hydrophobic liquid, and water containing plenty of surface-active agents. Mixing under the right conditions might create a gas cavity with a droplet core of a hydrophobic liquid, and a thin shell of surface-active agents. It is therefore of interest to understand, from a theoretical point of view, how antibubbles with encapsulations of Newtonian viscous fluids behave in a sound field. Increased understanding could lead to improved active leakage detection.

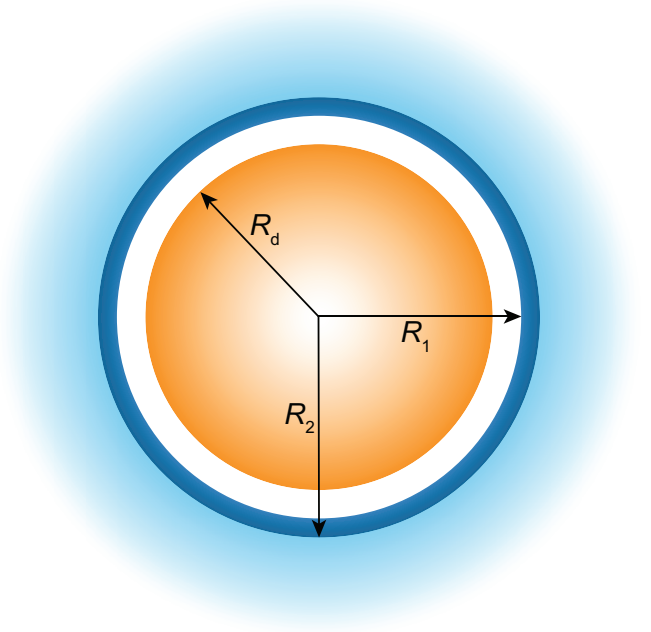

Fig. 1. Schematic of a liquid (light blue) containing an antibubble consisting of an oil core (brown) of radius R_d, surrounded by a gas layer (white), and a thin shell (dark blue) of inner radius R_1 and outer radius R_2.

Although many papers have been written on the dynamic behaviour of free and encapsulated microbubbles, especially on ultrasound contrast agents [4], only one paper has been published on acoustically active antibubbles [5]. Here the term microbubbles is defined as gas bubbles with a diameters less than 10 μm.

In our previous study, we treated antibubbles without an encapsulating shell [5]. In this study, we derive the dynamics of antibubbles encapsulated by a viscous shell, similar to the framework used for a viscoelastic solid shell [6], and for a Maxwell fluid shell [7]. Both the theory for a finite thickness shell, and the immediate approximation to a zero-thickness shell are presented.

II. Theory

Consider an antibubble as presented in Figure 1, where R_1, and R_2 are the instantaneous radii of the bubble from the centre of the bubble to the two interfaces, and R_d is the radius of the droplet inside the bubble. As this liquid droplet core can be considered incompressible, R_d is assumed to be constant when the bubble undergoes oscillations. The antibubble is surrounded by a shell layer of surface-active material. Both

Manuscript received December 8, 2014; revised January 13, 2015. This study has been supported by the by the Statoil-UiB Akademiaavtalen and The Michelsen Centre for Industrial Measurement Science and Technology.

K. Johansen and M. Postema are with the Department of Physics and Technology, University of Bergen, Allégaten 55, 5007 Bergen, Norway, e-mail: michiel.postema@ift.uib.no

S. Kotopoulis is with National Centre for Ultrasound in Gastroenterology, Haukeland University Hospital, Jonas Lies vei 65, 5021 Bergen, Norway.

ISBN: 978-988-19253-9-8
ISSN: 2078-0958 (Print); ISSN: 2078-0966 (Online)

the fluid composing the shell and the outer surrounding liquid are assumed to be viscous and incompressible. Assuming no mass exchange between the respective interfaces, the radial velocity $u(r,t)$ in the shell and in the surrounding fluid at a distance r from the centre of the bubble can be expressed as [8]:

$$u(r,t) = \frac{R_1^2}{r^2}\dot{R}_1 \ , \tag{1}$$

where $\dot{R}_1$ is the radial velocity of the bubble wall at interface 1. If $R_1 < r < R_2$, $u(r,t)$ denotes the velocity inside the shell; if $r > R_2$, $u(r,t)$ denotes the radial velocity of the surrounding liquid. From the assumption of an incompressible shell it can be shown that

$$R_2^3 - R_1^3 = R_{20}^3 - R_{10}^3 \ , \tag{2}$$

and

$$R_1^2\dot{R}_1 = R_2^2\dot{R}_2 \ , \tag{3}$$

where R_{10} and R_{20} are the respective equilibrium radii of the antibubble at rest.

From conservation of radial momentum [9], it follows that

$$\rho_{\mathrm{S}}\left(\frac{\partial u}{\partial t} + u\frac{\partial u}{\partial r}\right) = -\frac{\partial p}{\partial r} + \frac{\partial \tau_{rr}^{\mathrm{S}}}{\partial r} + \frac{3\tau_{rr}^{\mathrm{S}}}{r} \ , \tag{4}$$

and

$$\rho_{\mathrm{L}}\left(\frac{\partial u}{\partial t} + u\frac{\partial u}{\partial r}\right) = -\frac{\partial p}{\partial r} + \frac{\partial \tau_{rr}^{\mathrm{L}}}{\partial r} + \frac{3\tau_{rr}^{\mathrm{L}}}{r} \ , \tag{5}$$

where ρ_{S} is the the density of the shell, ρ_{L} is the density of the surrounding liquid, p is the pressure in the shell or the liquid, τ_{rr}^{S} is the viscous stress tensor in the shell, and τ_{rr}^{L} is the viscous stress in the liquid. Equation (4) is integrated from R_1 to R_2, and (5) is integrated from R_2 to infinity, substituting (1) for u. It is here assumed that the contribution to the radial momentum from the gas inside the cavity can be neglected. Combining these two integrals, result can be expressed as

$$\begin{aligned}
&\rho_{\mathrm{S}}R_1\ddot{R}_1\left[1+\left(\tfrac{\rho_{\mathrm{L}}-\rho_{\mathrm{S}}}{\rho_{\mathrm{S}}}\right)\tfrac{R_1}{R_2}\right] \\
&+\rho_{\mathrm{S}}\dot{R}_1^2\left[\tfrac{3}{2}+\left(\tfrac{\rho_{\mathrm{L}}-\rho_{\mathrm{S}}}{\rho_{\mathrm{S}}}\right)\times\left(\tfrac{4R_2^3-R_1^3}{R_2^3}\right)\right] \\
&\quad = P_{\mathrm{S}}(R_1,t) - P_{\mathrm{S}}(R_2,t) + P_{\mathrm{L}}(R_2,r) \\
&\quad\quad +\tau_{rr}^{\mathrm{S}}(R_2,t) - \tau_{rr}^{\mathrm{S}}(R_1,t) - \tau_{rr}^{\mathrm{L}}(R_2,t) \\
&\quad\quad +3\int_{R_1}^{R_2}\frac{\tau_{rr}^{\mathrm{S}}}{r}dr + 3\int_{R_2}^{\infty}\frac{\tau_{rr}^{\mathrm{L}}}{r}dr \ ,
\end{aligned} \tag{6}$$

where $P_{\mathrm{S}}(R_1,t)$ and $P_{\mathrm{S}}(R_2,t)$ are the pressures in the shell at interface 1 and 2, respectively, $P_{\mathrm{L}}(R_2,t)$ is the pressure in the liquid at interface 2, $\tau_{rr}^{\mathrm{S}}(R_1,t)$ and $\tau_{rr}^{\mathrm{S}}(R_2,t)$ are the stresses at interface 1 and 2, respectively, and $\tau_{rr}^{\mathrm{L}}(R_2,t)$ is the stress in the liquid at interface 2.

The boundary conditions from conservation of radial momentum can be stated as

$$P_{\mathrm{g}}(R_1,t) + \tau_{rr}^{\mathrm{S}}(R_1,t) = P_{\mathrm{s}}(R_1,t) + \frac{2\sigma_1}{R_1} \tag{7}$$

and

$$\begin{aligned}
P_{\mathrm{S}}(R_2,t) - \tau_{rr}^{\mathrm{S}}(R_2,t) &= P_{\mathrm{L}}(R_2,t) - \tau_{rr}^{\mathrm{L}}(R_2,t) \\
&\quad + \frac{2\sigma_2}{R_2} + P_{\mathrm{ac}}(t) \ ,
\end{aligned} \tag{8}$$

where $P_{\mathrm{g}}(R_1,t)$ is the instantaneous pressure inside the antibubble, P_{ac} is the pressure equal to the sum of the hydrostatic pressure P_0 and the instantaneous driving pressure at the position of the antibubble, and σ_1 and σ_2 are the surface tensions at the two respective interfaces. Combining (6) with the boundary conditions in (7) and (8) yields

$$\begin{aligned}
&\rho_{\mathrm{S}}R_1\ddot{R}_1\left[1+\left(\tfrac{\rho_{\mathrm{L}}-\rho_{\mathrm{S}}}{\rho_{\mathrm{S}}}\right)\tfrac{R_1}{R_2}\right] \\
&+\rho_{\mathrm{S}}\dot{R}_1^2\left[\tfrac{3}{2}+\left(\tfrac{\rho_{\mathrm{L}}-\rho_{\mathrm{S}}}{\rho_{\mathrm{S}}}\right)\times\left(\tfrac{4R_2^3-R_1^3}{R_2^3}\right)\right] \\
&\quad = P_{\mathrm{g}}(R_1,t) - \tfrac{2\sigma_1}{R_1} - \tfrac{2\sigma_2}{R_2} - P_0 \\
&\quad\quad -P_{\mathrm{ac}}(t) + 3\int_{R_1}^{R_2}\frac{\tau_{rr}^{\mathrm{S}}}{r}dr + 3\int_{R_2}^{\infty}\frac{\tau_{rr}^{\mathrm{L}}}{r}dr \ .
\end{aligned} \tag{9}$$

Let us assume a pressure change in the surrounding fluid under adiabatic conditions inside the bubble

$$p_{\mathrm{g}0}V_0^{\gamma} = p_{\mathrm{g}}V^{\gamma} \ , \tag{10}$$

where $p_{\mathrm{g}0}$ is the initial gas pressure, V_0 is the initial volume of the gas, γ is the polytropic exponent of the gas, p_{g} is the instantaneous gas pressure, and V is the instantaneous gas volume. From Figure 1 it is evident that the instantaneous pressure inside the antibubble can be expressed as

$$p_{\mathrm{g}} = p_{\mathrm{g}0}\left(\frac{R_{10}^3 - R_{\mathrm{d}}^3}{R_1^3 - R_{\mathrm{d}}^3}\right)^{\gamma} \ . \tag{11}$$

It now remains to determine the two integrals in (9). Knowing that $\tau_{rr} = 2\eta(\partial u/\partial r)$ is the shear viscous stress in a Newtonian fluid. Now, the last integral which describes the viscous stresses in the surrounding liquid, it can be expressed as

$$3\int_{R_2}^{\infty}\frac{\tau_{rr}^{\mathrm{L}}}{r}dr = -4\eta_{\mathrm{L}}\frac{R_1^2}{R_2^3}\dot{R}_1 \ , \tag{12}$$

where η_{L} is the shear viscosity in the surrounding liquid. The remaining integral describes the shear viscosity in the Newtonian fluid shell, and it can be expressed as

$$3\int_{R_1}^{R_2}\frac{\tau_{rr}^{\mathrm{S}}}{r}dr = -4\eta_{\mathrm{S}}\frac{(R_2^3 - R_1^3)}{R_1R_2^3}\dot{R}_1 \ . \tag{13}$$

Substituting (11) for the gas pressure inside the antibubble, the expression for the shear viscosity in surrounding liquid (12), and the fluid shell (13), a Rayleigh-Plesset-like equation for an antibubble with a Newtonian shell of finite thickness surrounded by a Newtonian viscous liquid can be found:

$$\begin{aligned}
&\rho_{\mathrm{S}}R_1\ddot{R}_1\left[1+\left(\tfrac{\rho_{\mathrm{L}}-\rho_{\mathrm{S}}}{\rho_{\mathrm{S}}}\right)\tfrac{R_1}{R_2}\right] \\
&+\rho_{\mathrm{S}}\dot{R}_1^2\left[\tfrac{3}{2}+\left(\tfrac{\rho_{\mathrm{L}}-\rho_{\mathrm{S}}}{\rho_{\mathrm{S}}}\right)\times\left(\tfrac{4R_2^3-R_1^3}{R_2^3}\right)\right] \\
&\quad = p_{\mathrm{g}0}\left(\tfrac{R_{10}^3-R_{\mathrm{d}}^3}{R_1^3-R_{\mathrm{d}}^3}\right)^{\gamma} - \tfrac{2\sigma_1}{R_1} - \tfrac{2\sigma_2}{R_2} - P_0 \\
&\quad\quad -4\eta_{\mathrm{L}}\frac{R_1^2}{R_2^3}\dot{R}_1 - 4\eta_{\mathrm{S}}\frac{(R_2^3 - R_1^3)}{R_1R_2^3}\dot{R}_1 - P_{\mathrm{ac}}(t) \ .
\end{aligned} \tag{14}$$

From (14) it can be seen from the first term on the left-hand side that the acceleration increases if $\rho_{\mathrm{L}} > \rho_{\mathrm{S}}$, and the acceleration decreases if $\rho_{\mathrm{L}} < \rho_{\mathrm{S}}$. The ratios of the densities effects the second term on the left-hand side in a similar way, decreasing and increasing the degree of nonlinearity. The first

ISBN: 978-988-19253-9-8
ISSN: 2078-0958 (Print); ISSN: 2078-0966 (Online)

term on the right-hand side is a different form of a Rayleigh-Plesset-like equation, describing the radial pulsation of a gas bubble. With a relatively large core droplet size, the pressure inside an antibubble will be larger than in a gas bubble under the same conditions. This makes it possible to predict that antibubbles should have a larger maximum excursion, and a different frequency-content in the oscillations compared to a gas bubble with no load.

From (14) it is possible to go from a finite shell thickness to a zero-thickness shell approximation. This is of interest in our study as the layer of surface-active material constituting the shell should be thin compared to R_1. Letting $R_2 \to R_1$, $\rho_S \to \rho_L$, and $\sigma = \sigma_1 + \sigma_2$, the zero-thickness approximation can be expressed as

$$R\ddot{R} + \tfrac{3}{2}\dot{R}^2 = \tfrac{1}{\rho_L}\left[P_{g0}\left(\tfrac{R_0 - R_d}{R - R_d}\right)^{\gamma} - \tfrac{2\sigma}{R} - P_0 - P_{ac} - 4\eta_L\frac{\dot{R}}{R} - 12\eta_S R_S\frac{\dot{R}}{R^2}\right] , \quad (15)$$

where R is the instantaneous radius, $\dot{R}$ and $\ddot{R}$ is the instantaneous radial velocity and acceleration of the shell boundary, respectively, R_0 is the equilibrium radius, and $R_S = R_2 - R_1$ is the shell thickness.

For a small excursion ξ of an antibubble, an analytic solution exists if $R_0\xi$ is small. Assuming $R = R_0(1 + \xi)$, where $\xi \ll 1$, (15) can be expressed as a second-order differential equation of the known form

$$\ddot{\xi} + \delta_T\dot{\xi} + \omega_0^2\xi = -\frac{P_{ac}(t)}{\rho_L R_0} , \quad (16)$$

where $\delta_T = \delta_{\eta_S} + \delta_{\eta_L}$ is the total damping constant, and ω_0 is the linear natural resonance frequency:

$$\delta_T = \frac{12R_S\eta_S}{\rho_L R_0^3} + \frac{4\eta_L}{\rho_L R_0^2} , \quad (17)$$

where the first term on the right-hand side is the viscous damping constant from the shell δ_{η_S}, and the second term is the viscous damping constant from the surrounding liquid δ_{η_L}. For a zero-thickness encapsulation R_S is on the order of 2–7 nm.

The linear natural resonance frequency can be expressed as

$$\omega_0^2 = \frac{1}{R_0^2\rho_L}\left[\frac{3\gamma p_{g0}}{1 - \left(\frac{R_d}{R_0}\right)^3} - \frac{2\sigma}{R_0}\right] . \quad (18)$$

It can be observed that the linear natural resonance frequency is augmented by the cubic ratio of the droplet core radius and the initial radius. It can be predicted that the behaviour of antibubbles compared to gas bubbles is highly similar for $R_d \to 0$ as $(R_d/R_0)^3 \to 0$, and opposite for large R_d, $(R_d/R_0)^3 \to 1$ resulting in a different behaviour of the antibubble to that of gas bubbles under the same conditions. If an antibubble is pulsating, it resonates with a linear damped resonance frequency ω_d, which is given by

$$\omega_d^2 = \frac{1}{R_0^2\rho_L}\left[\frac{3\gamma p_{g0}}{1 - \left(\frac{R_d}{R_0}\right)^3} - \frac{2\sigma}{R_0} - \frac{4\eta_L^2}{R_0^2\rho_L} - \frac{36\eta_S^2 R_S^2}{R_0^4\rho_L}\right] . \quad (19)$$

Both the viscous surrounding liquid and the viscous shell decrease the linear damped resonance frequency if the respective viscosities are increased.

III. Methods

The Rayleigh-Plesset-like equation (15) was solved numerically to simulate the radial dynamics of an antibubble and a gas bubble, both with and without a Newtonian viscous shell. An equilibrium bubble diameter of 100 μm was chosen. A single excitation pulse consisting of a sine-wave burst of 13 cycles at 500 kHz was used. Peak-negative acoustic pressures of 100 kPa (low), and 300 kPa (high) were evaluated. These acoustic pressures were chosen to match the acoustic conditions acceptable in underwater acoustics [10]. For antibubbles with a Newtonian viscous shell, (15) was solved 61 times, where core droplet size was varied between $0.6R_0$(low) and $0.9R_0$(high). This was done for each acoustic pressure, making it possible to study trends in the radial dynamics using colour surface plots. The respective simulations, at both pressures, are accompanied by a spectrogram to study trends in the frequency-content as a function of core droplet size. Computations were performed using the ode45 Runga-Kutta algorithm in MATLAB® 2014a (The Mathworks, Inc., Natick, MA, USA). The following fixed parameters were used: $P_0 = 30$ atm equivalent to the hydrostatic pressure at 300 m depth, $\gamma = 1.4$, $\eta_L = 1.0$ mPa s, $\eta_S = 1.2$ Pa s, $\rho_L = 1027$ kg/m^3, and $\sigma = 0.072$ N/m, $R_S = 2$ nm. Frequency spectra of the radius-time curves were computed using the FFT algorithm in MATLAB®. Linear colour interpolation was used to smoothen the plot appearance.

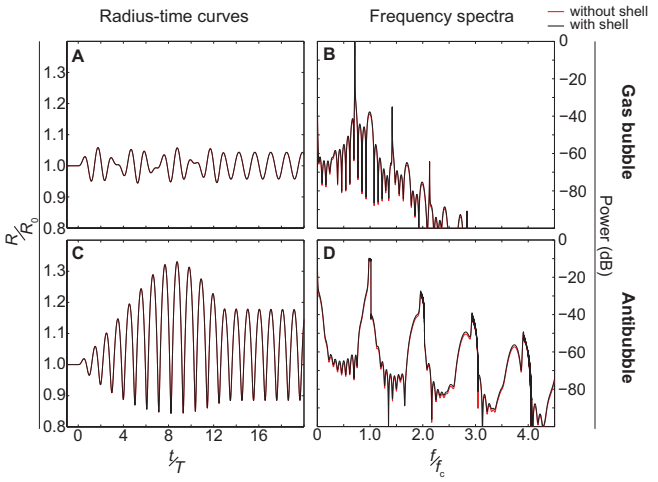

Fig. 2. Radius-time curves and their respective frequency spectra for an antibubble and a gas bubble, both with a Newtonian viscous shell (black) and without a shell (red). The radius of the core droplet $R_d = 0.8R_0$.The peak-negative acoustic pressure applied was 300 kPa. Bubble radii have been normalised to the equilibrium bubble radius; time has been normalised to the period T of the transmitted ultrasound; frequencies have been normalised to the centre frequency f_c of the transmit pulse.

IV. Results and Discussion

Figure 2 shows radius-time curves and frequency spectra of an antibuble and a gas bubble, both with and without a Newtonian viscous shell, during and after ultrasonic excitation at peak-negative acoustic pressures of 300 kPa. A core droplet

ISBN: 978-988-19253-9-8
ISSN: 2078-0958 (Print); ISSN: 2078-0966 (Online)

radius of 80 μm was chosen, equal to 80% of the equilibrium gas bubble radius. According to (19), the resonance frequency of the antibubble is equal to the centre frequency transmitted, 500 kHz, whereas the resonance frequency of the gas bubble is substantially lower, 350 kHz. Owing to this difference in resonance frequency, the radial excursion of the antibubble is a factor 1.3 greater than that of the gas bubble. Furthermore, Figure 2A and Figure 2B show interference of the bubble resonance frequency and the driving frequency.

As the red and black lines inidicate the behaviour of bubbles and antibubbles with and without a shell, it is evident the influence of the shell is negligible for bubbles of such large sizes. This is confirmed by the overlapping curves in Figure 2. It is also noted, that the antibubble and the gas bubble oscillations are hardly damped by the presence of this zero-thickness shell and the surrounding viscous liquid. From (17) it follows, that both the viscous damping by the shell and the surrounding liquid are of less influence for greater bubbles, as the respective damping terms are proportional to $1/R_0^2$ and $1/R_0^3$.

As the liquid core is assumed incompressible, the radial excursions of the antibubble must be highly asymmetric at higher acoustic amplitudes, as seen in Figure 2C. These asymmetric oscillations generate strong higher harmonics, as confirmed by Figure 2D. Owing to the presence of these higher harmonics in the acoustic response, antibubble detection should be feasible using harmonic imaging methods.

Figure 3 shows an overview of all simulations at 100 kPa. To clarify how to interpret Figure 3A we added cross sections, B and C, simulated at 80% and 65% core droplet radius, respectively. Analogously, in the frequency spectrogram shown in Figure 3D, we added cross sections at the same core droplet radii. From Figure 3A it can be seen, that the oscillation phase of the antibubble with respect to the incident sound wave is dependent of the core droplet radius, which can be attributed to differences between the resonance frequency of each antibubble and the sonication frequency [11]. Around resonant size, inertial growth and collapse can be observed from the wide red bands interlaced with narrow blue bands. At larger core droplet radii and smaller core droplet radii, a more linear oscillation regime is observed, as depicted by the equal thickness bands. At 65% core droplet radius, phase changes can be seen after 6 and 12 cycles. These can be explained by interference of

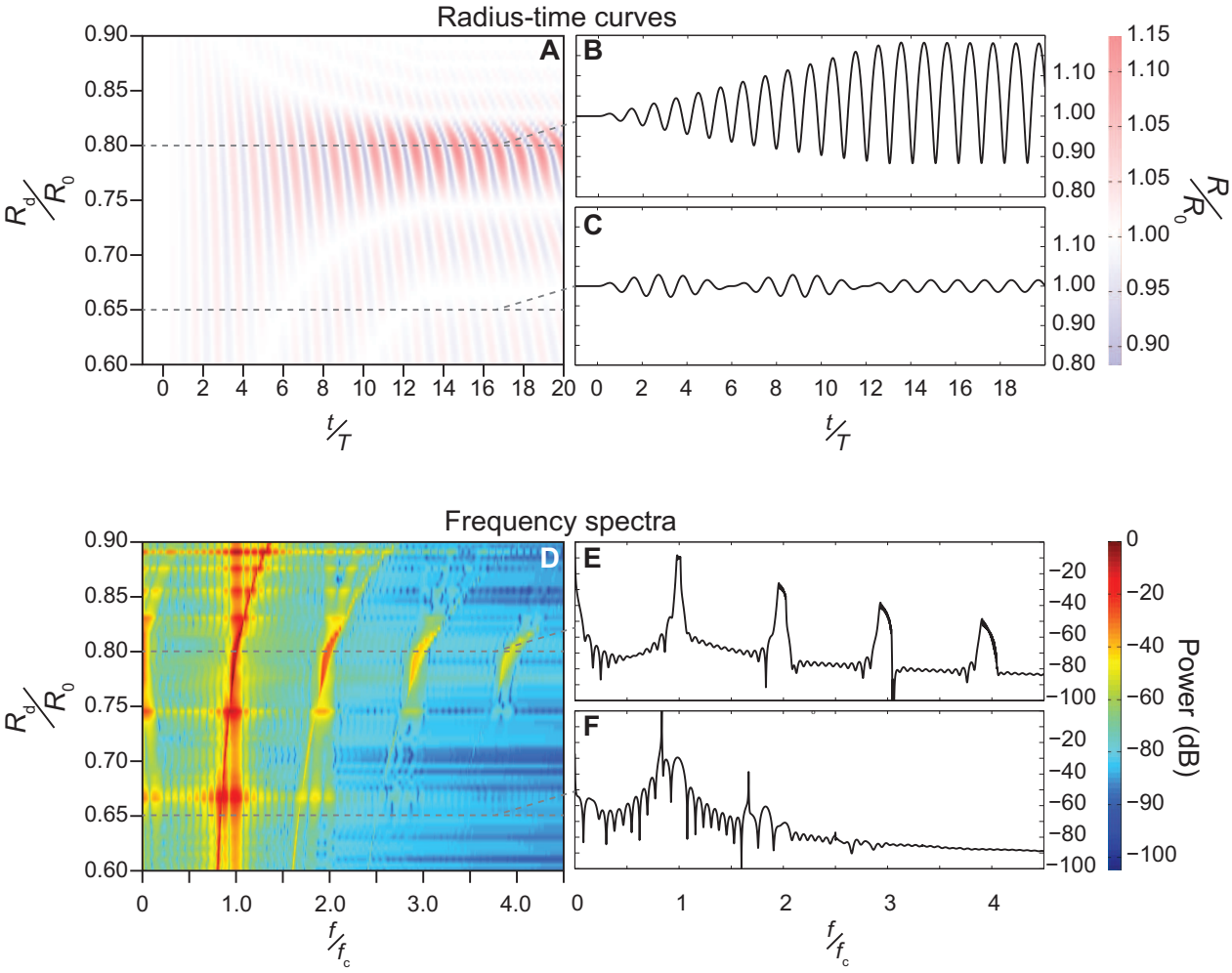

Fig. 3. Radius-time curves for an antibubble with a Newtonian viscous shell as a function of core droplet radius and sonication time in A with respective cross sections, B and C; radius-time curves in A have been transformed to frequency spectra in D, creating a spectrogram of instantaneous antibubble radius as a function of core droplet radius with respectiv cross sections, E and F. The peak-negative acoustic pressure applied was 100 kPa. Bubble radii have been normalised to the equilibrium radius; core droplet radii have been normalised to equilibrium radius; time has been normalised to the period of the transmitted ultrasound; frequencies have been normalised to the centre frequency of the transmit pulse.

ISBN: 978-988-19253-9-8
ISSN: 2078-0958 (Print); ISSN: 2078-0966 (Online)

the bubble resonance frequency and the driving frequency. From Figure 3F it can be appreciated that an antibubble with a 65% core droplet radius has a stronger response at its own resonance frequency than at the driving frequency. Around 80% core droplet radius, strong higher harmonics can be observed in the spectrogram of Figure 3D, whereas at core droplet sizes much greater or much less, the nonlinear content is limited to the second harmonic. If an antibubble is subjected to high acoustic amplitudes, the bubble response is highly nonlinear, independent of core droplet size. This is demonstrated by the spectrogram in Figure 4, which was simulated at a peak-negative acoustic pressure of 300 kPa. Even at the lowest core droplet radii, third harmonics were observed.

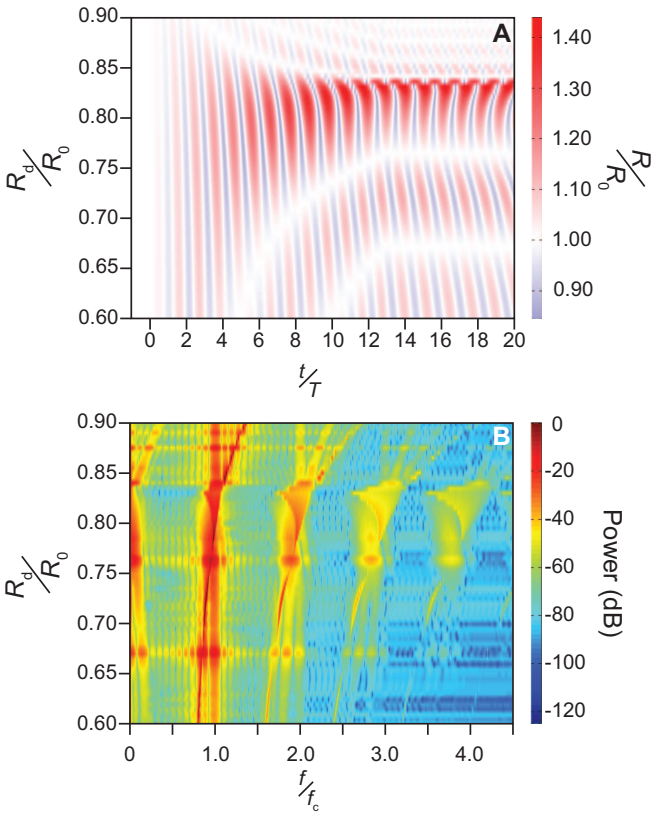

Fig. 4. Radius-time curves for an antibubble with a Newtonian viscous shell as a function of core droplet radius and sonication time in A and its corresponding spectrogram in B. The peak-negative acoustic pressure applied was 300 kPa. Bubble radii have been normalised to the equilibrium radius; time has been normalised to the period of the transmitted ultrasound; frequencies have been normalised to the centre frequency of the transmit pulse.

V. Conclusion

From our simulations we see that the resonance frequency of antibubbles strongly depends on the core droplet size. In addtion, the contribution to the radial dynamics from a zero-thickness Newtonian viscous shell is negligible for bubbles of the size studied.

The oscillation phase with respect to the incident sound wave is dependent on the antibubble core droplet size. At high enough acoustic amplitudes, antibubbles oscillate highly nonlinearly independent of core droplet size. This may allow for active leakage detection and differentiation using harmonic imaging methods.

References

[1] J. Moreno-Trejo, R. Kumar, and T. Markeset, "Mapping factors influencing the selection of subsea petroleum production systems: a case study," *International Journal of System Assurance Engineering and Management*, vol. 3, no. 1, pp. 6–16, 2012.

[2] D. L. Miller, "Ultrasonic detection of resonant cavitation bubbles in a flow tube by their second-harmonic emissions," *Ultrasonics*, vol. 19, no. 5, pp. 217–224, 1981.

[3] S. Dorbolo, H. Caps, and N. Vandewalle, "Fluid instabilities in the birth and death of antibubbles," *New Journal of Physics*, vol. 5, no. 161, pp. 1–9, 2003.

[4] A. A. Doinikov and A. Bouakaz, "Review of shell models for contrast agent microbubbles." *IEEE Transactions on Ultrasonics, Ferroelectrics, and Frequency Control*, vol. 58, no. 5, pp. 981–993, 2011.

[5] S. Kotopoulis, K. Johansen, O. H. Gilja, A. T. Poortinga, and M. Postema, "Acoustically active antibubbles," *Acta Physica Polonica A*, 2015, in press.

[6] C. C. Church, "The effects of an elastic solid surface layer on the radial pulsations of gas bubbles," *J. Acoust. Soc. Am.*, vol. 97, no. 3, pp. 1510–1521, 1995.

[7] A. A. Doinikov and P. A. Dayton, "Maxwell rheological model for lipid-shelled ultrasound microbubble contrast agents." *J. Acoust. Soc. Am.*, vol. 121, no. 6, pp. 331–3340, 2007.

[8] T. G. Leighton, *The Acoustic Bubble*. Academic Press, London, 1994.

[9] L. D. Landau and E. M. Lifshitz, *Fluid Mechanics*, 2nd ed. Butterworth-Heineman, Oxford, 1987.

[10] Office of the Federal Register (U S), *Code of Federal Regulations, Title 50, Wildlife and Fisheries, PT. 200-599, Revised as of October 1, 2010*. Government Printing Office, Washington, DC, 2011.

[11] M. Postema and G. Schmitz, "Ultrasonic bubbles in medicine: influence of the shell," *Ultrasonics Sonochemistry*, vol. 14, no. 4, pp. 438–444, 2007.

ISBN: 978-988-19253-9-8
ISSN: 2078-0958 (Print); ISSN: 2078-0966 (Online)